A new algorithm for using Pb isotopes to determine the provenance of bullion in ancient Greek coinage

Francis Albarede, Gillan Davis, Janne Blichert-Toft, Liesel Gentelli, Haim Gitler, Marine Pinto, Philippe Telouk

A new algorithm for using Pb isotopes to determine the provenance of bullion in ancient Greek coinage

Francis Albarede[1], Gillan Davis[2], Janne Bichert-Toft[1], Liesel Gentelli[1], Haim Gitler[3], Marine Pinto[1], Philippe Telouk[1]

[1] *Ecole Normale Supérieure de Lyon, 69007 Lyon, France*
[2] *Australian Catholic University, National School of Arts, North Sydney, NSW 2060*
[3] *Israel Museum, Jerusalem*

Abstract. A new algorithm is proposed that uses Pb isotopes to help identify the ore deposits utilized as sources of silver in Antiquity. The algorithm takes natural and analytical isotope fractionation into account. It proposes a statistical measure of the distances between the Pb isotope compositions of ores and artifacts. This measure is amenable to statistical tests at any confidence level. The new algorithm is applied to the Pb isotope compositions of the end-members derived from 368 new Pb isotope data on silver coinage minted between the late 6th to late 2nd centuries BCE and presented in Albarede et al. (submitted). The algorithm identifies the local sources expected for the mints associated with major silver ores found in the territories of Athens, Thasos, and Thrace, while demonstrating that Thrace, Northern Macedonia, and Chalkidiki supplied notable amounts of bullion to Aegina and Ptolemaic Egypt. Minor proportions of what we are designating an old Sardinian ‘mix' created by long-distance trade was used by archaic Athens, Corinth, and Aegina. Various islands in the Cyclades (Siphnos, Keos, Seriphos) also appear to be early contributors to archaic Corinthian and Macedonian silver. The present study clearly demonstrates that recycled and mixed use of bullion by mints formed a substantial part of their silver stocks. The new algorithm warrants more detailed Pb isotopic studies of well-dated coinage to document the changing nature of silver fluxes over time.

Introduction

Assigning metal provenance to a coin or artifact using lead isotopes has met with some criticisms, mostly on the basis of statistical arguments (Budd et al., 1996, Budd et al., 1993), but has nevertheless become a standard tool of archeology and numismatics (Killick et al., 2020). In principle, the method is simple: the lead isotope composition of the artifact in question is compared with the Pb isotope data from large databases tabulating the Pb isotope compositions of ores. Despite its apparent simplicity, there are a number of issues with this approach: (1) given the intensive search for precious metal ore throughout past millennia, silver in a given artifact is probably different from what can be sampled today, since the silver ore that was used has been completely exhausted and hence is not included in any Pb isotope ore database; (2) low-temperature processes, such as precipitation, hydrothermal alteration, and weathering cause variability of lead isotopic abundances in ores in the permille range; (3) the yields of lead purification by ion-exchange chromatography carried out prior to analysis by mass spectrometry may be < 100%, leading to erroneous (i.e. fractionated) measured Pb isotope compositions; and (4) variable evaporation and ionization in the mass spectrometer used for isotopic analysis may, if not adequately corrected for, misrepresent the natural abundances (mass bias). Effects 2-4 are known as mass-dependent fractionation (also referred to as the

'isotopic effect'), which implies that the changes in relative isotope abundances induced by these effects vary linearly with mass. For example, the relative bias on the $^{208}Pb/^{204}Pb$ ratio (atomic mass difference of four) is twice the relative bias on the $^{206}Pb/^{204}Pb$ ratio (atomic mass difference of two).

The equations describing the linear mass fractionation effect are as follows (Hofmann, 1971):

$$\begin{aligned} x_1 &= \left(\frac{^{206}\mathrm{Pb}}{^{204}\mathrm{Pb}}\right)_{meas} = \left(\frac{^{206}\mathrm{Pb}}{^{204}\mathrm{Pb}}\right)_0 (1 + 2\,f) \\ x_2 &= \left(\frac{^{207}Pb}{^{204}Pb}\right)_{meas} = \left(\frac{^{207}\mathrm{Pb}}{^{204}\mathrm{Pb}}\right)_0 (1 + 3\,f) \\ x_3 &= \left(\frac{^{208}\mathrm{Pb}}{^{204}\mathrm{Pb}}\right)_{meas} = \left(\frac{^{208}\mathrm{Pb}}{^{204}\mathrm{Pb}}\right)_0 (1 + 4\,f) \end{aligned} \qquad (1)$$

in which the '0' subscript denotes the ratio before fractionation, *meas* stands for the measured ratio after fractionation, and *f* is a variable fractionation factor typically of the order of 0.001. This set of equations (1) represents a straight-line going through the unfractionated unknown point labelled '0' in equation set (1) in the three-dimensional space of lead isotopes. A linear model of mass-dependent fractionation is assumed but an exponential fractionation law would not lead to a noticeably different conclusion in the present context.

The linear mass fractionation effect is depicted in Fig. 1, in which the ^{204}Pb-normalized isotopic ratios of a set of 253 lead ores collected in the Aegean realm by (Stos-Gale et al., 1996) are represented. As shown by the theoretical straight-line calculated from Eqns. 1, multiple groups of points show strong mass-dependent trends (Fig. 1). This point was previously made by Albarède et al. (2020) and for the peri-Aegean galena ores by Vaxevanopoulos et al. (2022a). As visible from Fig. 4 of the latter work, the apparent spread of legacy data typified by the OXALID (Stos-Gale et al., 1996, Stos-Gale and Gale, 2009) and the IBERLID (de Madinabeitia et al., 2021) is significantly larger than the spread of modern Pb isotope data acquired by multiple-collection inductively-coupled plasma mass spectrometry (MC-ICP-MS), for which instrumental mass bias is far better controlled and corrected for than legacy data acquired by thermal ionization mass spectrometry (TIMS). This observation suggests that the spread of legacy data may be due more to inefficient correction of both chemical fractionation and instrumental mass bias by TIMS than to effects of low-temperature geological processes. The quest for the provenance of silver artifacts must, therefore, be modified by keeping in mind that ore Pb isotopic abundances are fractionated following the mass-dependent law of Eqns. 1 (Fig. 1). This quest is the topic of the present work, which will, at least to some extent, alleviate the isotopic fractionation issues of databases such as OXALID. A new algorithm is described that solves the mass-fractionation conundrum. Together with the approach to bullion mixing investigated in Albarède et al. (submitted), this algorithm allows a major step forward to assess the provenance of silver coins and artifacts from Pb isotopes. Its implementation on the Pb isotope compositions of the end-members obtained by Albarède et al. (submitted) for the coinages of Athens, Corinthia, Aegina, Thasos, Thrace, Macedonia, and Ptolemaic Egypt illustrates a new potential of Pb isotopes as a provenance tracer.

Figure 1

The second point emphasized in the present work deals with the concept of distance in the 3-dimensional space of Pb isotope compositions. The conventional 'Euclidian' distance between two points $\vec{x}$ and $\vec{x}'$ in this space:

$$d = \sqrt{(x_1 - x_1')^2 + (x_2 - x_2')^2 + (x_3 - x_3')^2} \quad (1)$$

(Birch et al., 2020, Sayre et al., 1992, Stos-Gale and Gale, 2009) does not take into account the statistical errors on the data. Scaling by standard deviation has been applied more recently by Rodriguez et al. (2023). Simple scaling does not, however, account for the strong correlation between errors on ^{204}Pb-normalized ratios due to the small signal on this isotope (Albarède et al., 2004), a problem which was addressed by weighing the data by the full covariance matrix **W** of the Pb standard isotope reference material NIST 981 (Albarède et al., 2020, Delile et al., 2014, Westner et al., 2020)

$$d = \sqrt{(\vec{x} - \vec{x}')^T \mathbf{W}^{-1} (\vec{x} - \vec{x}')} \quad (2)$$

in which the superscript T indicates the transpose vector. We see that calculating the Euclidian distance implicitly assumes a covariance matrix **W** equal to unity. With Rodriguez et al.'s (2023) AMALIA algorithm, the diagonal terms of **W** are different from each other and the off-diagonal terms (correlation coefficients) are equal to zero, which is inconsistent with general analytical evidence.

A new algorithm for provenance identification

Figure 2

The distance taken into account is the distance d_i of the point representing the artifact to the mass-dependent fractionation line going through the point representing the *i*-th ore considered as a potential source of bullion (Fig. 2). As long as the Pb isotope ratios of an artifact under consideration and any Pb ore from the database differ by no more than the first decimal, their respective fractionation lines can be considered parallel, which leads to some simplification of the formulas. Distance d_i was computed by projecting $\overrightarrow{\Delta X_i} = (\vec{x}_i - \vec{x}_0)$, the 3-dimensional vector joining the points representing the lead isotopic ratios of the artifact

$$\vec{x}_0 = [(^{206}\mathrm{Pb}/^{204}\mathrm{Pb})_0, (^{207}\mathrm{Pb}/^{204}\mathrm{Pb})_0, (^{208}\mathrm{Pb}/^{204}\mathrm{Pb})_0] \quad (3)$$

and of the *i*-th ore

$$\vec{x}_i = [(^{206}\mathrm{Pb}/^{204}\mathrm{Pb})_i, (^{207}\mathrm{Pb}/^{204}\mathrm{Pb})_i, (^{208}\mathrm{Pb}/^{204}\mathrm{Pb})_i] \quad (4)$$

on the plane *P* perpendicular to the mass-dependent fractionation line *D* with direction vector

$$\vec{v} = [2(^{206}\mathrm{Pb}/^{204}\mathrm{Pb})_0, 3(^{207}\mathrm{Pb}/^{204}\mathrm{Pb})_0, 4(^{208}\mathrm{Pb}/^{204}\mathrm{Pb})_0] \quad (5)$$

In this expression, the digits correspond to the difference in atomic mass of each Pb isotope involved in the ratio. Defining $\vec{n} = \vec{v}/\|\vec{v}\|$ as the unit vector along the mass fractionation line, the distance d_i is equal to:

$$d_i = \left\| \overrightarrow{\Delta X_i} \times \vec{n} \right\| \quad (6)$$

where the operator × stands for the vector cross-product. The expression accounting for different mass-fraction lines for the artifact and the ore, due to widely different Pb isotope compositions, would be slightly more convoluted but of much less practical interest. The fractionation factor *f* between the ore and the artifact is obtained from the projection $f\vec{n}$ of $\overrightarrow{\Delta X}$ on the same mass-fractionation line:

$$f_i = \overrightarrow{\Delta X_i} \cdot \vec{n} \quad (7)$$

where the dot symbol · stands for the dot product.

In order to obtain dimensionless distances, we first define the error matrix **W** as:

$$\mathbf{W} = \begin{bmatrix} 2sx_x^* & 0 & 0 \\ 0 & 3sx_y^* & 0 \\ 0 & 0 & 4sx_z^* \end{bmatrix} \begin{bmatrix} 1 & 0.96 & 0.94 \\ 0.96 & 1 & 0.96 \\ 0.94 & 0.96 & 1 \end{bmatrix} \begin{bmatrix} 2sx_x^* & 0 & 0 \\ 0 & 3sx_y^* & 0 \\ 0 & 0 & 4sx_z^* \end{bmatrix} \quad (8)$$

where the first and last matrices are the diagonal standard-deviation matrices with

$$x^* = \left[x_x^*, x_y^*, x_z^*\right] \quad (9)$$

standing for the common Pb isotope composition (Albarede and Juteau, 1984, Stacey and Kramers, 1975). The mass-fractionation factor is taken as $s = 0.001$. Note the non-zero off-diagonal correlation coefficients, which greatly enhance the distance *d*. The intermediate correlation matrix is the noise correlation matrix (Albarède et al., 2004). The squared distances $|d|^2$ are normalized to the 2-dimensional shadow of **W** on the same plane (see Supplement 5A in (Johnson and Wichern, 2002). This requires finding two orthogonal vectors perpendicular to $\vec{n}$, which can be achieved by Gram-Schmidt orthogonalization. Since the weighing matrix is derived from the Pb isotope reference material measurements and not from the data set itself, this metric is not a proper Mahalanobis distance. The normalized squared distances $|d|^2$ now follow a chi-squared distribution with two degrees of freedom and a 95% confidence value of 5.99 (critical distance). In other words, an ore with a Pb isotope composition leading to a $|d|^2$ value in excess of 5.99 can be rejected as significantly different from the artifact in question. The data with distances less than this critical value will hereinafter be referred to as 'hits'.

An example of fit is provided for the high-$^{206}Pb/^{204}Pb$ end-member of Athens' data set presented by Albarède et al. (submitted) with only the data with the smallest *d* values shown for clarity (Fig. 3). The closest 64 ores with a distance to this end-member shorter than the critical value will be retained. As expected from the original assumptions, the data conspicuously spread along the mass-dependent fractionation lines.

Figure 3

Provenance of lead from Greek and Ptolemaic Egypt silver coinage

Albarède et al. (submitted) addressed the issue of mixed bullion used to mint silver coins from Athens, Corinthia, Aegina, Thasos, Thrace, Macedonia, and Ptolemaic Egypt (Table 1). The power-law distribution of the first principal component observed for each data set led us to conclude that a binary mixture accounts for most of the data and that the end-members were different for each data set. A fit of the first principal component by an exponential distribution allowed the calculation of the Pb isotope compositions of the two end-members for all the issues and the results are listed in Table 1.

Set	*n*	$^{206}Pb/^{204}Pb_a$	$^{207}Pb/^{204}Pb_a$	$^{208}Pb/^{204}Pb_a$	$^{206}Pb/^{204}Pb_b$	$^{207}Pb/^{204}Pb_b$	$^{208}Pb/^{204}Pb_b$
Athens	112	18.101	15.605	38.135	18.874	15.700	38.923
Corinth	56	17.855	15.581	37.863	18.803	15.683	38.852
Aegina	18	18.165	15.589	38.115	18.755	15.676	38.830
Thasos	38	18.379	15.646	38.464	18.793	15.679	38.882
Thrace	50	18.215	15.624	38.146	18.800	15.683	38.926
Macedonia	48	18.308	15.630	38.358	18.870	15.691	38.951
Ptolemies	46	18.027	15.593	37.954	18.748	15.675	38.852

Table 1. Reproduction of the results obtained by Albarède et al. (submitted)*. The symbol n refers to the number of coins analyzed. Labels a and b refer to the end-members computed from the power-law distribution of the data along the mixing line controlled by the first principal component. For convenience, these end-members will be referred to as the low- and high-$^{206}Pb/^{204}Pb$ end-members, respectively.*

We then used the method described above to assess the potential provenance of each end-member involved in the bullion used to mint the local coinage. The color scale on the right-hand side of each map indicates that the darker the color, the more likely the end-member in question is to represent the ore source. The data will be discussed in the order of the low-$^{206}Pb/^{204}Pb$ end-member first, and the high $^{206}Pb/^{204}Pb$ end-member second. The localities are indicated as outcomes of the algorithm but should always be assessed in conjunction with archaeological and numismatic evidence.

1. Athens

The description of this data set was given by Albarède et al. (submitted) and will not be repeated here. Figure 4a shows that the only significant hit of the low-$^{206}Pb/^{204}Pb$ end-member is located in the Iglesiente province of Sardinia, a point discussed in detail below. With Sardinia being part of the continental margin pulled out from the Southern European coast between Catalonia and Provence during the Cenozoic (Jolivet and Faccenna, 2000, Schettino and Turco, 2011), sources in Southern Gaul must also be considered together with Iglesiente. This low-$^{206}Pb/^{204}Pb$ end-member is only present in small amounts in the bullion representing a small subset of the coins.

Figures 4a and 4b

Figure 4b is consistent with the dominant, high-$^{206}Pb/^{204}Pb$ end-member corresponding to the Laurion mines. Chios and Taurus provide single hits which deserve further investigations centered on the dating of the coins.

2. Corinth

As for Athenian coinage, the most likely source of the low-$^{206}Pb/^{204}Pb$ end-member is located in Sardinia (Fig. 5a). The provenance of the high-$^{206}Pb/^{204}Pb$ end-member is less evident (Fig. 5b). The Hercynian Northern Sardinia may have provided Pb but is not known for silver ores (Boni et al., 1996). Ancient literature does not mention modern Tunisia or Western Crete but they are possible silver sources (Treister, 1996). The islands of Kythnos in the Cyclades and Euboea also represent possible sources.

Figures 5a and 5b

3. Aegina

This data set is small and hence all provenance assessment should be considered with caution. The source of the low-$^{206}Pb/^{204}Pb$ end-member most likely is located in Southwestern Sardinia (Fig. 6a). Disregarding single hits in Northern Sardinia, Taurus, and undocumented ores in the Alps, the sources of the high-$^{206}Pb/^{204}Pb$ end-member likely are located in Rhodope, Mount Pangaion, and Kavala and Skra, in Northern Macedonia (Fig. 6b). Herodotus (3.57) describes the silver mines of Siphnos as very active in the second half of the 6th c. BCE down to their abrupt end at c. 525 BCE (Sheedy et al., 2020, Treister, 1996). However, the present samples of Aeginetan coins do not show the significant contribution of ores from this island postulated by Kraay and Emeleus (1962), Gentner et al. (1978), and Pernicka and Wagner (1985), contra Stos-Gale and Davis (2020). In contrast, the relatively high gold contents of many of these coins pointed out by Gentner et al. (1980) strongly reinforces the present findings that Thrace and North Macedonia were major contributors to the bullion.

Figures 6a and 6b

4. Thasos

Again, this data set is relatively small. No multiple hits with small *d* values are found for the low-$^{206}Pb/^{204}Pb$ end-member (Fig. 7a) with the possible exception of the Parnon mountains in Southeastern Peloponnese. Geology does not support silver sources in Ionia nor in the Peloponnese. This inconclusive search of an end-member only questions a minor contribution to the mixed bullion. Unlike the Sardinian end-member identified above, the source(s) of geologically old Pb involved in Thasos coinage do not emerge from the noise. The lack of resolution on this end-member likely reflects the geological complexity of low-$^{206}Pb/^{204}Pb$ sources located in Northern Greece and the Balkans (Zagorchev et al., 2017): tectonically old Pb bullion is present but in small quantities, and its provenance cannot be unambiguously identified.

Figures 7a and 7b

In contrast, as suggested by Pernicka et al. (1981) and Stos-Gale and Davis (2020), the island of Thasos itself is the probable source of the predominant high-$^{206}Pb/^{204}Pb$ end-member (Fig. 7b). Nevertheless, Phrygia and Mysia ores cannot be formally excluded. Kythnos island is known for copper smelting in the Bronze Age (Stos-Gale, 1989), but not as a major source of silver ore (Treister, 1996).

5. Thrace

This geographic term includes coinage from all the city-states east of the Strymon river and includes Thasos. Again, the provenance of the low-$^{206}Pb/^{204}Pb$ end-member is not identified by the search (Fig. 8a). In contrast, the provenance of the high-$^{206}Pb/^{204}Pb$ end-member is well constrained with ores most likely produced in Thasos and Eastern Chalkidiki (Figure 8b). As with Thasian coinage, the island of Kythnos and Thessaly, which are better known for bronze artifacts (Treister, 1996), are also potential sources. Thracian sources are conspicuously absent.

Figures 8a and 8b

6. Macedonia

The provenance of the low-$^{206}Pb/^{204}Pb$ end-member is ambiguous (Fig. 9a). Two hits in Paeonia or Illyria are not inconsistent with the early history of Macedonia, but the small number of these hits is insufficient to draw a conclusion. This ambiguity may explain why bullion sources in the Pangaion and other more northerly regions with protracted geological history do not define a valid end-member. The outcome for the high-$^{206}Pb/^{204}Pb$ end-member is much stronger. The clear hits on Keos and Seriphos (Fig. 9b), especially for the coins minted after Greece was subjugated by Philip II (see Albarède et al., (submitted), Fig. S3), confirms the contribution of these islands to silver production in the Aegean as late as the 4th c. BCE (Vaxevanopoulos et al., 2022a).

Figures 9a and 9b

7. Ptolemaic Egypt

Again, the low-$^{206}Pb/^{204}Pb$ end-member cannot be securely located (Fig. 10a). In contrast, the= hits identified for the high-$^{206}Pb/^{204}Pb$ end-member are much clearer with ore sources in eastern=and western Thrace (Fig. 10b). As suggested by Fig. S3 in Albarède et al. (submitted), input of=Thracian silver may be a windfall from the first Syrian War (274–271 BCE).

Figures 10a and 10b

Data set	component 1 (low-$^{206}Pb/^{204}Pb$)	component 2 (high-$^{206}Pb/^{204}Pb$)
Athens	Sardinia	Laurion
Corinthia	Sardinia	Kythnos and Euboea
Aegina	Sardinia	Thrace and N Macedonia
Thasos	Parnon?	Thasos, and Phrygia+ Mysia
Thrace	-	Thasos, E Chalkidiki, Kythnos
Macedonia	Peonia?	Keos and Seriphos
Ptolemies	-	Thrace

Table 2. Major hits and other probable provenances of the end-members of the bullion used to mint silver coinage in the Greek world (late 6th c. to late 4th c. BCE). The localities are visible on the maps in the Supplemental Material.

Discussion and concluding remarks

(Note to the editor: the 3 paragraphs in red have been added to meet the reviewers' suggestion. Delete this note for type-setting)

Allocation should always be done with caution, in particular for small mining fields such as Kythnos (Stos-Gale, 1998) in the Aegean, and Euboea: veins may have been mined over the centuries to the last mineral of ore and slag heaps may have been obliterated by later human activity. Despite extensive research, the memory of some deposits and their locations may have been lost with time (Vaxevanopoulos et al., 2022a). An additional hurdle is the existence of mixed bullion, a problem addressed in detail by Albarède et al. (submitted). A single sample that generates no hits over large distances may be suspected to be a mixture of different sources of bullion. Groups of samples, such as hoards (Eshel et al., 2019, Eshel et al., 2021 , Gentelli et al., 2021), or broadly scattered hits associated with a single issue, such as alexanders or sigloi, can be handled with the convex hull technique (Blichert-Toft et al., 2022) with some success.

It has been suggested that Ag isotopes may help confirm whether a particular ore field has been used to produce bullion (Milot et al., 2022, Vaxevanopoulos et al., 2022b): if the $^{109}Ag/^{107}Ag$ ratio of an ore falls in the very narrow range defined by silver coinage (±1 part per 10,000), it is legitimate to accept that this particular field is a potential source of bullion. But the absence of proof is not proof of absence: the lack of coinage-like $^{109}Ag/^{107}Ag$ ratios in a particular district is not sufficient in itself to disqualify it as a possible source. In such cases, alternative sources of information, such as literature and archaeometallurgy, judicially used, should be preferred.

The strength of the present model is manifest in the results of two well-documented searches: Athenian silver coinage uses bullion from the Laurion, and Thasian silver coinage uses bullion from Thasos. Other inconclusive searches, in particular those concerning the low-$^{206}Pb/^{204}Pb$ end-members of Thasos (Fig. 7a), Thrace (Fig. 8a), Macedonia (Fig. 9a), and Ptolemaic Egypt (Fig. 10a), must be acknowledged. They likely reflect a protracted geological history of the sources in Northern Greece and the Balkans which may stretch over more than 400 million years. This geologically old end-member is only present in small quantities in the mixed bullion and resolution on the origin of this end-member is lost in the overall noise of the data. But even if the provenance of this old end-member cannot be unambiguously identified, the method seems efficient enough to backtrack the Pb isotope composition of the geologically young end-member and identify the potential source region.

The time scale considered for the present data sets does entail major approximations, but this work is more focused on presenting a novel approach to a new problem than on detailed numismatic studies. The results and their interpretation rest on data sets pooled over more than four centuries of minting and paves the way for more detailed and definitive studies. Investigating specific time windows and specific issues corresponding to well-documented events, such as the second Persian invasion, the Peloponnesian War, and the attempts of the Ptolemies to control Greece, would be certain to bring novel constraints on monetary fluxes in these troubled periods. Relative probability assessment using kernel density, as proposed by De Ceuster et al. (2020, 2023), but using the chi-squared distribution of distances rather than normal distributions on isotopic ratios, may improve the resolution of provenance in time and space. Kernels, however, assume a certain form of density distribution and the risk is to introduce information that does not exist in the raw data.

The new methods presented here use Pb isotopes in coinage to assess the provenance of silver flowing through the mints of major city-states (Athens, Corinth, Aegina, Thasos), ethnically

related entities (Thrace), and kingdoms (Macedonia and Ptolemaic Egypt). Because binary mixing is now taken into account, Pb isotopes can be used to combine a much-improved determination of the end-members entering bullion mixes (Albarède et al., (submitted) with the new algorithm developed here to identify the provenance of the end-members. When permitted by data coverage, notably in the case of Athens, the results allow for major changes in provenance and relative abundances of sources to be put into historical context. In particular, these new methods allow the data to probe the role of bullion recycling and its importance relative to fresh sources of metal.

The new complementary mixing and provenance algorithms are clearly validated by the cases in which local sources of silver are historically and archeologically attested. We confirm that (i) silver coinage from Athens contain a large component mined in the Laurion area, (ii) coinage from Thasos used bullion mined in Thasos, while (iii) Thracian coinage used Thraco-Macedonian resources. Lead isotopes logically reveal that city-states and kingdoms endowed with silver ore deposits included locally extracted bullion into the mix used to mint their own monetary issues, but that these local sources were complemented by foreign bullion. In the case of Athens, the state initially derived all its bullion from foreign sources before accessing bullion locally but continued to receive silver from abroad for many reasons including tribute, port fees and taxes, and trade as is historically attested. Others without domestic silver sources such as Corinth, Aegina, and Ptolemaic Egypt, could nevertheless acquire bullion and mint their own money. The silver supplied by revenues from tolls and trade (Corinth), tribute (Egypt), trade (Aegina) and all the foregoing (Athens) should be considered in further studies. Lead isotopes only inform us on ore sources, not on the pathways from the sources to the mints.

An intriguing question was raised in different forms by different authors (Bresson, 2019, Flament, 2019, Picard, 2007, Thür and Faraguna, 2018): how closely does the local bullion production of a city-state endowed with silver mines match the apparent monetary production? The effect of recycling has not so far been quantitatively evaluated, simply because the data are missing. For example, if older issues are recycled twice a year, money production appears doubled. If the mint of Athens recycled coinage predominantly produced from Laurion ores, the data cannot be used to compare silver yields from the mines of Laurion with monetary production. In this case, history and numismatics should be summoned to assess recycling practices, not to be confused with reuse through overstriking.

The present work assesses that Southwestern Sardinia was a significant source of early silver minted by Athens, Corinth, and Aegina (see Albarède et al., (submitted), Fig. S3). By no means should this conclusion be taken as evidence that silver mining activities in Sardinia was contemporaneous with minting in those city-states. The time of extraction remains unknown. A Sardinian ‘mix', analogous to the Persian ‘mix' described by Olivier et al. (2017) and Blichert-Toft et al. (2022) for sigloi and Alexanders, may have taken centuries to grow through trade, in particular by Phoenician or Greek merchants during a time when literary and epigraphic sources were disinterested in such questions and surviving evidence is sparse and fragmentary. The Sardinian mix may have also grown more quickly in the 6th c. BCE, which saw the number of shipwrecks at the bottom of the Mediterranean and adjacent seas surging (Parker, 1990), thereby demonstrating the remarkable expansion of long-haul trade. A Sardinian component is already present in hoards of *Hacksilber* dated from the Late Bronze and Early Iron Ages from the Levant (Eshel et al., 2019, Eshel et al., 2021, Gentelli et al., 2021). Since there is no solid archaeological evidence that silver was actually mined in Sardinia during the Archaic period, the present results only show that some sort of Sardinian mix was

going around the Mediterranean on Phoenician and other ships which reached Athens, Corinth, and Aegina. Additional sources isotopically similar to Sardinia, notably from Southern Gaul (Albarède et al., unpublished), which belongs to geological unit similar to those present in Sardinia, may have contributed to this mix.

Cycladic islands, notably Keos, Kythnos and Seriphos, for which factual and historical evidence is thin or lacking (Treister, 1996), appear as sources of bullion, in particular for Corinth and Macedonia. Such a mix is likely to have been short-lived and geographically restricted. The contribution of argentiferous ores from Siphnos, where mining activity was short-lived and declined at the end of the 6th c. BCE (Sheedy et al., 2020, Treister, 1996), does not show up in the present results.

Acknowledgements. This work is a contribution of Advanced Grant 741454-SILVER-ERC-2016-ADG 'Silver Isotopes and the Rise of Money' awarded to FA by the European Research Council. François de Callataÿ has been of great help with result interpretation. We thank François de Callataÿ and Johan van Heesch for granting access to the money collection of the Royal Library of Brussels. George Kakavas allowed access to the collection of the Numismatic Museum of Athens. Elena Kontou and her group are thanked for help during sampling. We also acknowledge with thanks access to the collections of The Israel Museum in Jerusalem. We thank two anonymous reviewers and Editor Marcos Martinón-Torres for very useful comments.

References

Albarede, F., Davis, G., Gentelli, L., Bichert-Toft, J., Gitler, H., Pinto, M., Telouk, P., submitted. Bullion mixtures in silver coinage from ancient Greece and Egypt. Journal of Archaeological Science.Albarede, F., Juteau, M., 1984. Unscrambling the lead model ages, Geochim. Cosmochim. Acta 48, 207-212.

Albarede, F., Davis, G., Gentelli, L., Bichert-Toft, J., Gitler, H., Pinto, M., Telouk, P., submitted. Bullion mixtures in silver coinage from ancient Greece and Egypt, Journal of Archaelogical Science.

Albarède, F., Telouk, P., Blichert-Toft, J., Boyet, M., Agranier, A., Nelson, B., 2004. Precise and accurate isotopic measurements using multiple-collector ICPMS, Geochim. Cosmochim. Acta 68, 2725-2744.

Albarède, F., Blichert-Toft, J., Gentelli, L., Milot, J., Vaxevanopoulos, M., Klein, S., Westner, K., Birch, T., Davis, G., de Callataÿ, F., 2020. A miner's perspective on Pb isotope provenances in the Western and Central Mediterranean, Journal of Archaeological Science 121, 105194.

Birch, T., Kemmers, F., Klein, S., Seitz, H., Höfer, H., 2020. Silver for the Greek colonies: Issues, analysis and preliminary results from a large- scale coin sampling project, Metallurgy in numismatics 6.

Blichert-Toft, J., de Callataÿ, F., Télouk, P., Albarède, F., 2022. Origin and fate of the greatest accumulation of silver in ancient history, Archaeological and Anthropological Sciences 14, 1-10.

Boni, M., Balassone, G., Iannace, A., 1996. Base metal ores in the Lower Paleozoic of southwestern Sardinia.

Bresson, A., 2019. The Athenian Money Supply in the Late Archaic and Early Classical Period, The Journal of Ancient Civilizations 34, 135–153.

Budd, P., Haggerty, R., Pollard, A., Scalife, B., Thomas, R., 1996. Rethinking the quest for provenance, Antiquity 70, 168-174.

Budd, P.D., Gale, D., Pollard, A.M., Thomas, R.G., Williams, P.A., 1993. Evaluating lead isotope data: further ohservations, Archaeometry 35, 241-247.

De Ceuster, S., Degryse, P., 2020. A ‘match–no match ‘numerical and graphical kernel density approach to interpreting lead isotope signatures of ancient artefacts, Archaeometry 62, 107-116.
De Ceuster, S., Machaira, D., Degryse, P., 2023. Lead isotope analysis for provenancing ancient materials: a comparison of approaches, RSC advances 13, 19595-19606.
de Madinabeitia, S.G., Ibarguchi, J.G., Zalduegui, J.S., 2021. IBERLID: A lead isotope database and tool for metal provenance and ore deposits research, Ore Geology Reviews 137, 104279.
Delile, H., Blichert-Toft, J., Goiran, J.-P., Keay, S., Albarède, F., 2014. Lead in ancient Rome’s city waters, Proceedings of the National Academy of Sciences 111, 6594-6599.
Eshel, T., Erel, Y., Yahalom-Mack, N., Tirosh, O., Gilboa, A., 2019. Lead isotopes in silver reveal earliest Phoenician quest for metals in the west Mediterranean, Proceedings of the National Academy of Sciences 116, 6007-6012.
Eshel, T., Gilboa, A., Yahalom-Mack, N., Tirosh, O., Erel, Y., 2021. Debasement of silver throughout the Late Bronze–Iron Age transition in the Southern Levant: Analytical and cultural implications, Journal of Archaeological Science 125, 105268.
Flament, C., 2019. The Athenian Coinage, from Mines to Markets, The Journal of Ancient Civilizations 34, 189-209.
Gentelli, L., Blichert-Toft, J., Davis, G., Gitler, G., Gitler, H., Albarede, F., 2021. Metal provenance of Late Bronze to Iron Age Hacksilber hoards in the southern Levant, Joural of Archaeological Sciences 134, 105472.
Gentner, W., Müller, O., Wagner, G., Gale, N., 1978. Silver sources of archaic Greek coinage, Naturwissenschaften 65, 273-284.
Hofmann, A., 1971. Fractionation corrections for mixed-isotope spikes of Sr, K, and Pb, Earth Planet. Sci. Letters 10, 397-402.
Johnson, R.A., Wichern, D.W., 2002. Applied Multivariate Statistical Analysis, Prentice-Hall, Englewood Cliff.
Jolivet, L., Faccenna, C., 2000. Mediterranean extension and the Africa- Eurasia collision, Tectonics 19, 1095-1106.
Killick, D., Stephens, J., Fenn, T., 2020. Geological constraints on the use of lead isotopes for provenance in archaeometallurgy, Archaeometry 62, 86-105.
Kraay, C.M., Emeleus, V.M., 1962. The Composition of Greek Silver Coins: analysis by neutron activation, Ashmolean Museum, Oxford.
Milot, J., Blichert-Toft, J., Sanz, M.A., Malod-Dognin, C., 2022. Silver isotope and volatile trace element systematics in galena samples from the Iberian Peninsula and the quest for silver sources of Roman coinage, Geology 50.
Olivier, J., Duyrat, F., Carrier, C., Blet-Lemarquand, M., 2017. Minted Silver in the Empire of Alexander, Alexander the Great, a Linked Open World, Ausonius Éditions, pp. 127–146.
Parker, A., 1990. Classical antiquity: the maritime dimension, Antiquity 64, 335-346.
Pernicka, E., Gentner, W., Wagner, G., Vavelidis, M., Gale, N.H., 1981. Ancient lead and silver production on Thasos (Greece), ArchéoSciences, revue d'Archéométrie 1, 227-237.
Pernicka, E., Lutz, C., Bachmann, H.G., Wagner, G.A., Elitzsch, C., Klein, E., 1985. Alte Blei-Silber-Verhüttung auf Sifnos, Der Anschnitt, 185-199.
Picard, O., 2007. Monnaie et circulation monétaire à l'époque classique, Pallas, 113-128.
Rodríguez, J., Sinner, A.G., Martínez-Chico, D., Zalduegui, J.F.S., 2023. AMALIA, A Matching Algorithm for Lead Isotope Analyses: Formulation and proof of concept at the roman foundry of Fuente Spitz (Jaén, Spain), Journal of Archaeological Science: Reports 51, 104192.
Sayre, E., Yener, K.A., Joel, E., Barnes, I., 1992. Statistical evaluation of the presently accumulated lead isotope data from Anatolia and surrounding regions, Archaeometry 34, 73-105.

Schettino, A., Turco, E., 2011. Tectonic history of the western Tethys since the Late Triassic, Bulletin 123, 89-105.
Sheedy, K.A., Gore, D.B., Blet-Lemarquand, M., Davis, G., 2020. Elemental composition of gold and silver coins of Siphnos, in: Sheedy, K.A., Davis, G. (Eds.), Metallurgy in Numismatics 6: Mines, Metals and Money: Ancient World Studies in Science, Archaeology and History, Royal Numismatic Society Special Publications, London, pp. 149-163.
Stacey, J.S., Kramers, J.D., 1975. Approximation of terrestrial lead isotope evolution by a two-stage model, Earth Planet. Sci. Letters 26, 207-221.
Stos-Gale, Z., 1989. Cycladic copper metallurgy, Old World Archaeometallurgy, Der Anschnitt, Beiheft 7, 279-293.
Stos-Gale, Z., 1998. The role of Kythnos and other Cycladic islandsin the origins of Early Minoan metallurgy, in: Mendoni, L., Mazarakis-Ainian, A. (Eds.), Kea-Kythnos: history and Archaeology, de Boccard, Paris & Athens, pp. 717-736.
Stos-Gale, Z.A., Gale, N.H., Annetts, N., 1996. Lead isotope data from the Isotrace Laboratory, Oxford: archaeometry data base 3, ores from the Aegean, part 1, Archaeometry 38, 381-390.
Stos-Gale, Z.A., Gale, N.H., 2009. Metal provenancing using isotopes and the Oxford archaeological lead isotope database (OXALID), Archaeological and Anthropological Sciences 1, 195–213.
Stos-Gale, Z.A., Davis, G., 2020. The minting/mining Nexus: New understandings of Archaic Greek silver coinage from lead isotope analysis, in: Sheedy, K., Davis, G. (Eds.), Metallurgy in Numismatics 6: : Mines, Metals and Money: Ancient World Studies in Science, Archaeology and History, Royal Numismatic Society, London, pp. 87-100.
Thür, G., Faraguna, M., 2018. Silver from Laureion: Mining, Smelting, and Minting.
Treister, M.Y., 1996. The role of metals in ancient Greek history, Brill, Leiden.
Vaxevanopoulos, M., Blichert-Toft, J., Davis, G., Albarède, F., 2022a. New findings of ancient Greek silver sources, Journal of Archaeological Science 137, 105474.
Vaxevanopoulos, M., Davis, G., Milot, J., Blichert-Toft, J., Malod-Dognin, C., Albarède, F., 2022b. Narrowing provenance for ancient Greek silver coins using Ag isotopes and Sb contents of potential ores, Journal of Archaeological Science 145, 105645.
Wagner, G.A., Gentner, W., Gropengiesser, H., Gale, N.H., 1980. Early Bronze Age lead-silver mining and metallurgy in the Aegean: the ancient workings on Siphnos, Scientific studies in early mining and extractive metallurgy, pp. 63-85.
Westner, K.J., Birch, T., Kemmers, F., Klein, S., Höfer, H.E., Seitz, H.-M., 2020. Rome´s rise to power. Geochemical analysis of silver coinage from the Western Mediterranean (4th to 2nd centuries BCE), Archaeometry 62, 577-592.
Zagorchev, I., Balica, C., Kozhoukharova, E., Balintoni, I.C., 2017. Pirin metamorphic and igneous evolution revisited in a geochronological frame based on U-Pb zircon studies, Geologica balcanica 46, 27-63.

Figure Captions

Figure 1. Literature data on lead ores from the Cyclades, Laurion, and Thasos (Stos-Gale et al., 1996) in the 3-dimensional space of ^{204}Pb-normalized isotopic ratios. The spread predicted from linear mass-dependent fractionation (Eqns. 1) is represented for the Kithnos samples as a straight line, but most samples from the other localities also show a similar fractionation pattern.

Figure 2: Distance d between the composition of an artifact and the mass fractionation line inferred from the set of equations (1) for an ore sample in the 3-dimensional space of Pb isotope ratios. The direction vector of the mass-fractionation line D has the coordinates [2 $(^{206}Pb/^{204}Pb)_{meas}$, 3 $(^{207}Pb/^{204}Pb)_{meas}$, 4 $(^{208}Pb/^{204}Pb)_{meas}$]. $|\Delta\vec{X}|$ is the Euclidian distance. To avoid the effect of mass-dependent fractionation, which, regardless of its origin, is ubiquitous in ore data, the distance d is calculated in the plane P perpendicular to the mass-discrimination line. The length of the vector f is a measure of the apparent mass-dependent fractionation between the artifact and the ore. Color-filled error ellipsoids project themselves as 2-dimensional 'shadow' ellipses in the plane perpendicular to the mass-fractionation direction. The error ellipse is assumed to be the same for the artifact and for the ores.

Fig. 3. Ore deposits with Pb isotope compositions at the minimum distance from the high-$^{206}Pb/^{204}Pb$ end-member of Athens' data set (hits). Note the streaks caused by natural or analytical mass-dependent fractionation. The ellipse represents the uncertainties associated with mass-dependent fractionation. The open gray symbols represent the ca. 7000 Pb isotope compositions of galena ores tabulated in the Lyon database.

Fig. 4. Maps of isotopic hits (low-$^{206}Pb/^{204}Pb$, top, Fig. 4a) and (high-$^{206}Pb/^{204}Pb$, bottom, Fig. 4b), slightly jittered to improve legibility. Probable provenance of bullion used by Athens' mint (end of the 6th c. to end of the 4th c. BCE). The closed white circles show the occurrences of Pb ± Ag ores analyzed for Pb isotope compositions. The white cross shows the location of the mint (from https://nomisma.org), or that of the capital city of a region. The color scale to the right refers to the reduced distance d in the 3-dimensional space of ^{204}Pb-normalized Pb isotopes between the end-members derived from the mixing theory (Albarède et al., submitted) and each ore from the Lyon database. The darker the color, the shorter the distance between the Pb isotope composition of the end-member and the particular ore plotted on the map). Values in excess of 5.99 fall outside the 95% confidence level and can be ignored.

Fig. 5. Maps of isotopic hits (low-$^{206}Pb/^{204}Pb$, top, Fig. 5a) and (high-$^{206}Pb/^{204}Pb$, bottom, Fig. 5b). Probable provenance of bullion used by Corinth's mints. See caption to Fig. 4 for details. Silver sources in Tunisia and Northern Sardinia are not documented in surviving ancient sources.

Fig. 6. Maps of isotopic hits (low-$^{206}Pb/^{204}Pb$, top, Fig. 6a) and (high-$^{206}Pb/^{204}Pb$, bottom, Fig. 6b). Probable provenance of bullion used by Aegina's mint. See caption to Fig. 4 for details.

Fig. 7. Maps of isotopic hits (low-$^{206}Pb/^{204}Pb$, top, Fig. 7a) and (high-$^{206}Pb/^{204}Pb$, bottom, Fig. 7b). Probable provenance of bullion used by Thasos' mints. See caption to Fig. 4 for details.

Fig. 8. Maps of isotopic hits (low-$^{206}Pb/^{204}Pb$, top, Fig. 8a) and (high-$^{206}Pb/^{204}Pb$, bottom, Fig. 8b). Probable provenance of bullion used by Thracian mints. See caption to Fig. 4 for details. The low-$^{206}Pb/^{204}Pb$ end-member (Sardinia) is weakly localized.

Fig. 9. Maps of isotopic hits (low-$^{206}Pb/^{204}Pb$, top, Fig. 9a) and (high-$^{206}Pb/^{204}Pb$, bottom, Fig. 9b). Probable provenance of bullion used by Macedonia's mints. See caption to Fig. 4 for details.

Fig. 10. Maps of isotopic hits (low-$^{206}Pb/^{204}Pb$, top, Fig. 10a) and (high-$^{206}Pb/^{204}Pb$, bottom, Fig. 10b). Probable provenance of bullion used by Ptolemies' mints. See caption to Fig. 4 for details. The low-$^{206}Pb/^{204}Pb$ end-member (top) is poorly localized.

Figure 1

Click here to access/download;Figure;Fig.2-01 Cyclades.jpg

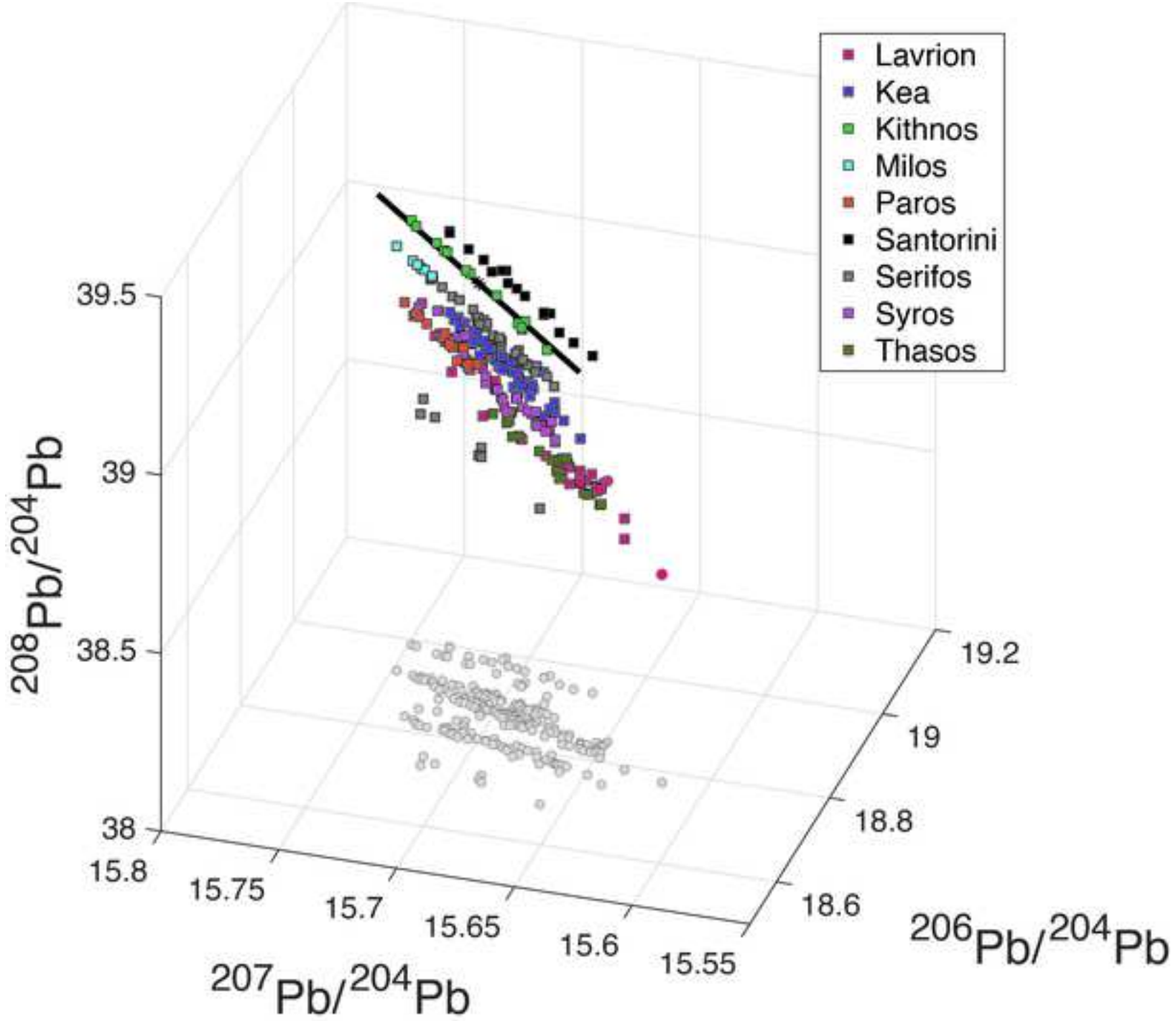

Figure 2

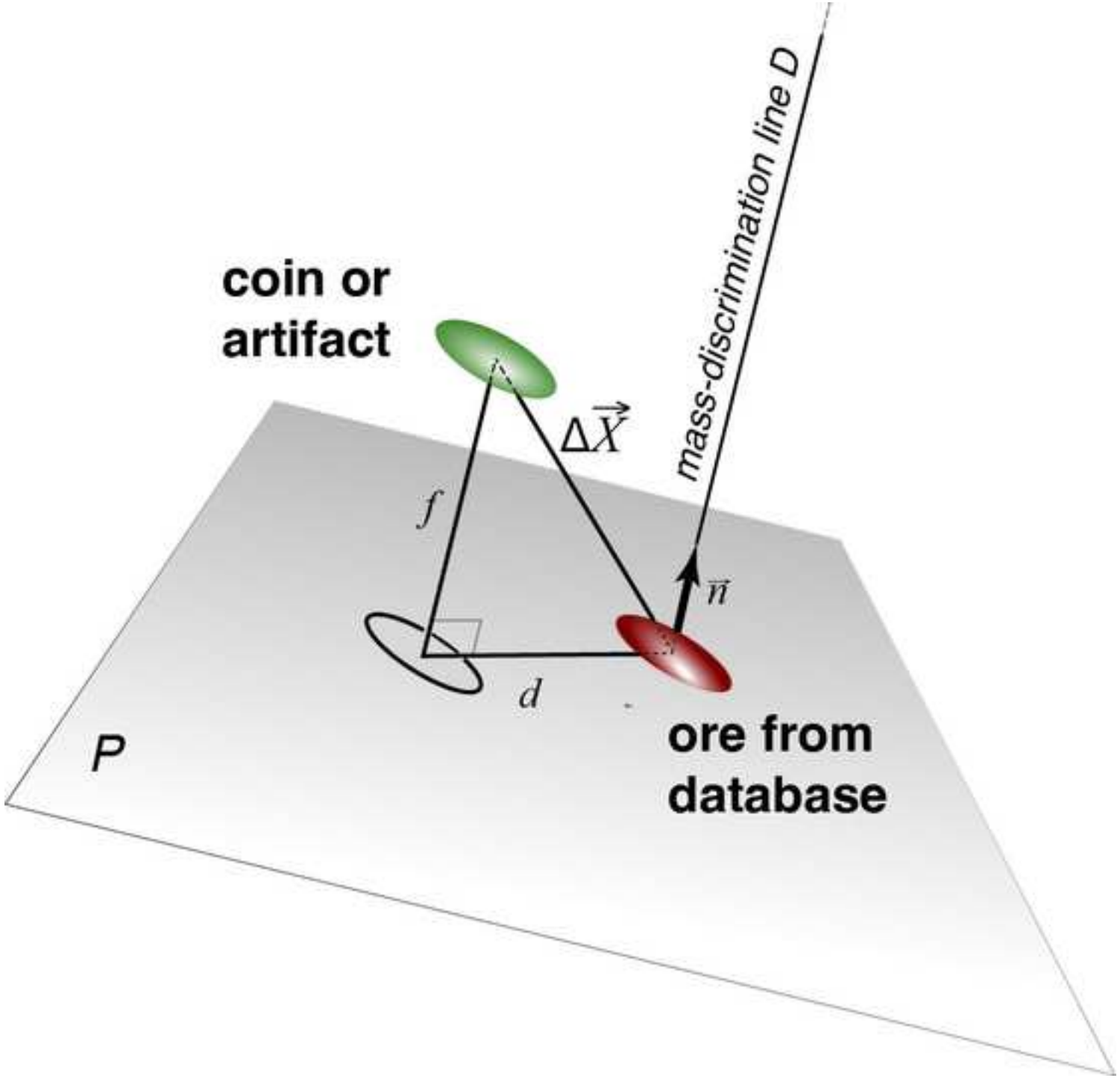

Figure 3

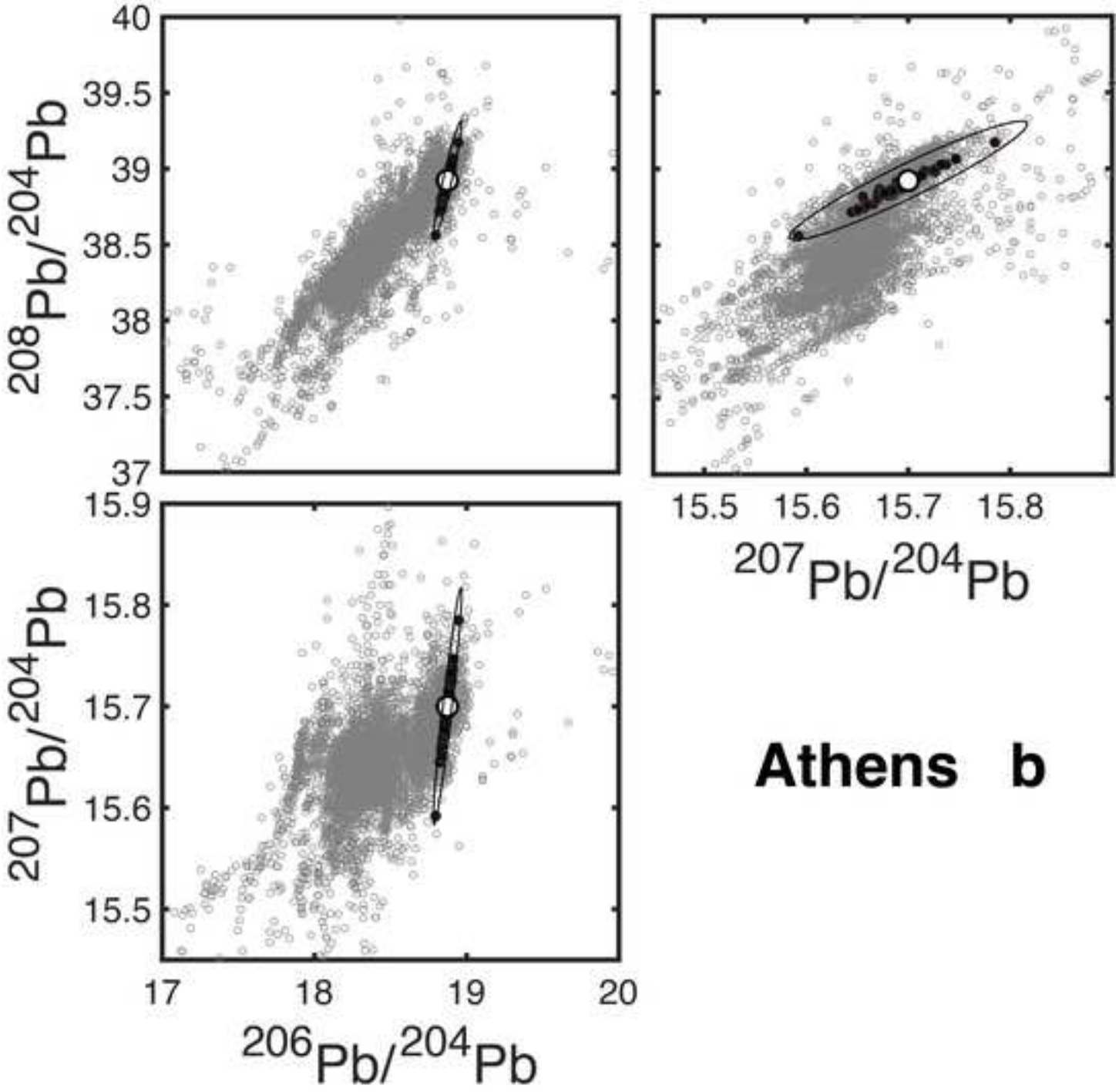

Figure 4a

Click here to access/download;Figure;Fig.2-04a Athens_map.jpg

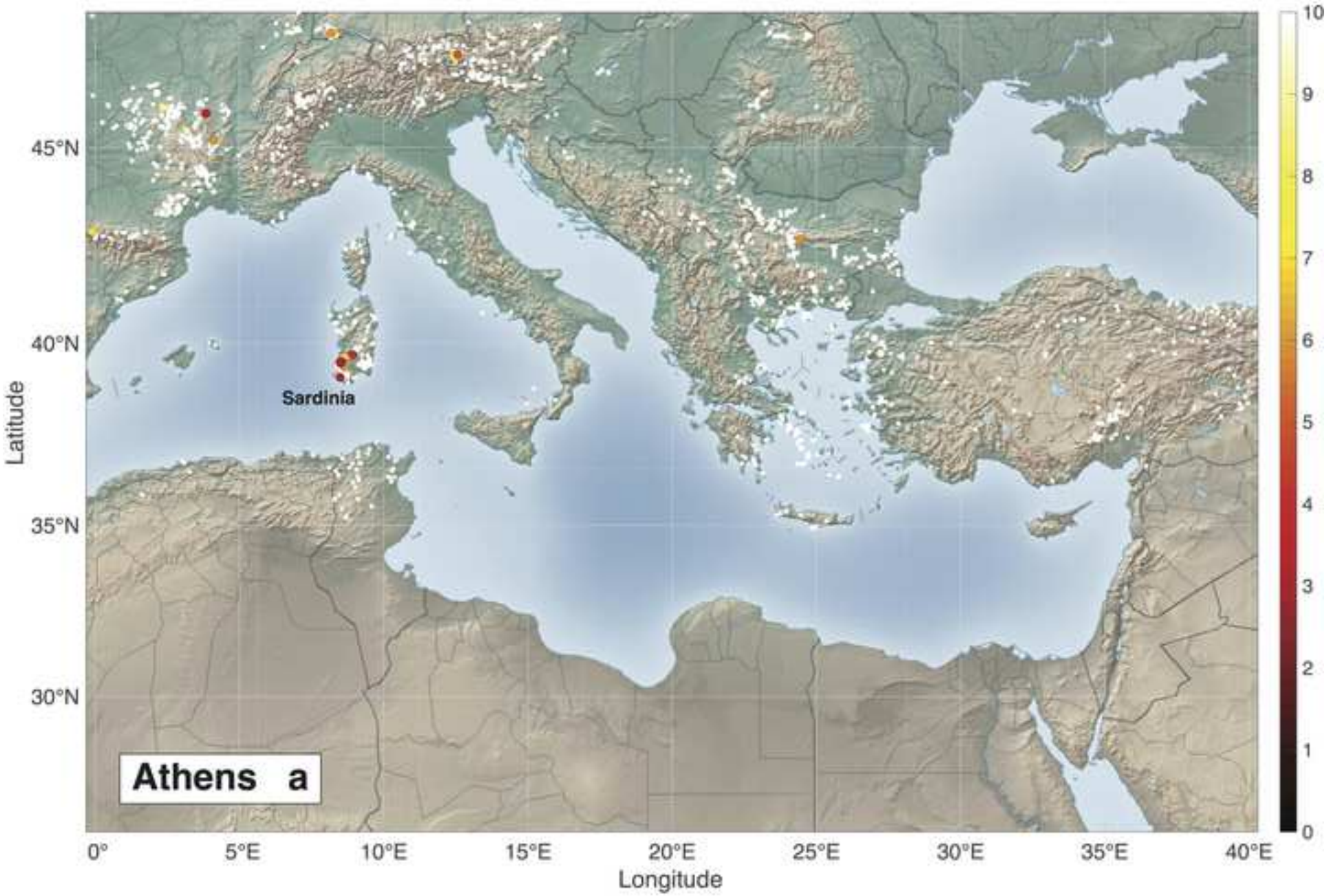

Figure 4b

Click here to access/download;Figure;Fig.2-04b Athens_map.jpg

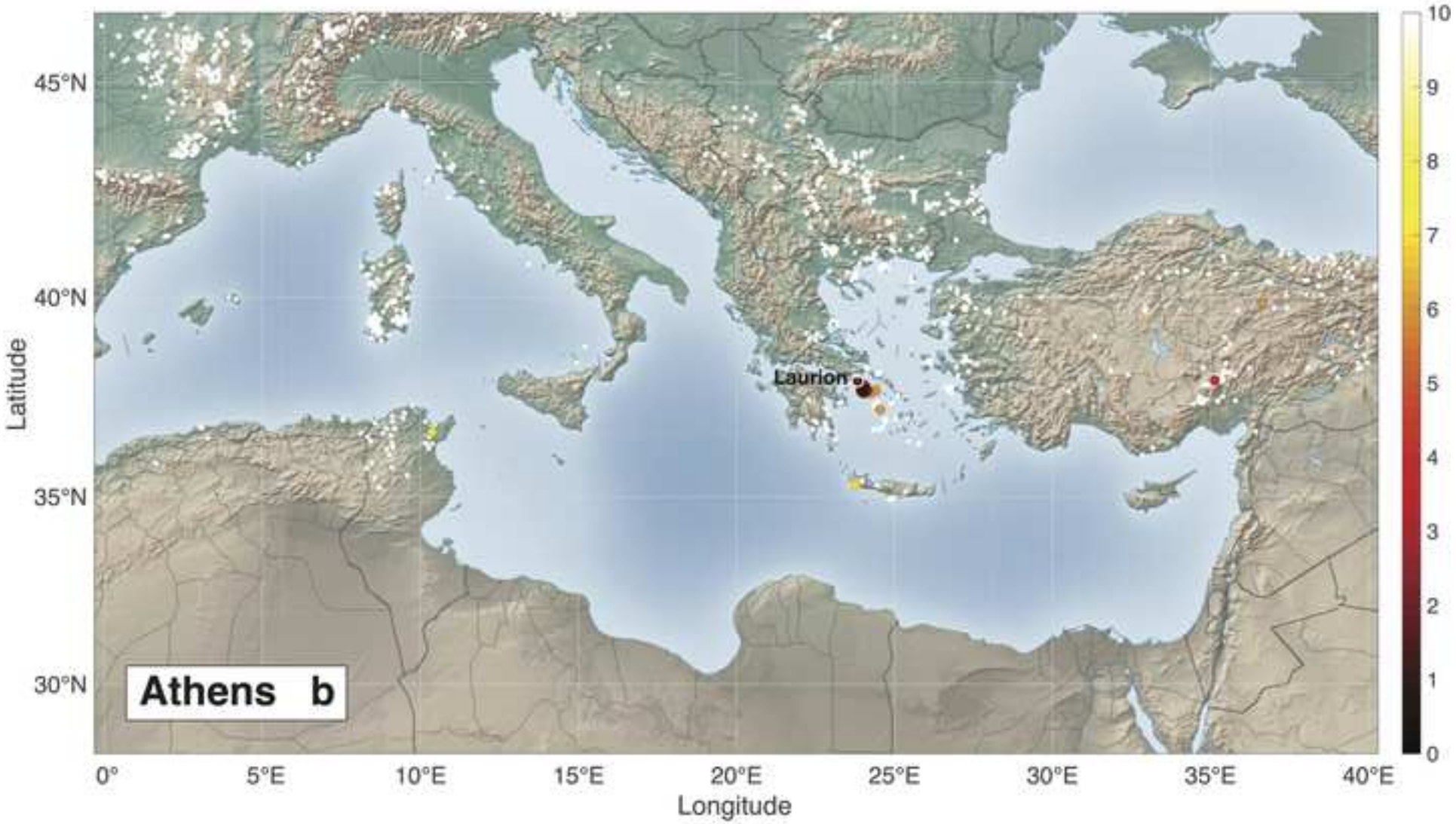

Figure 5a

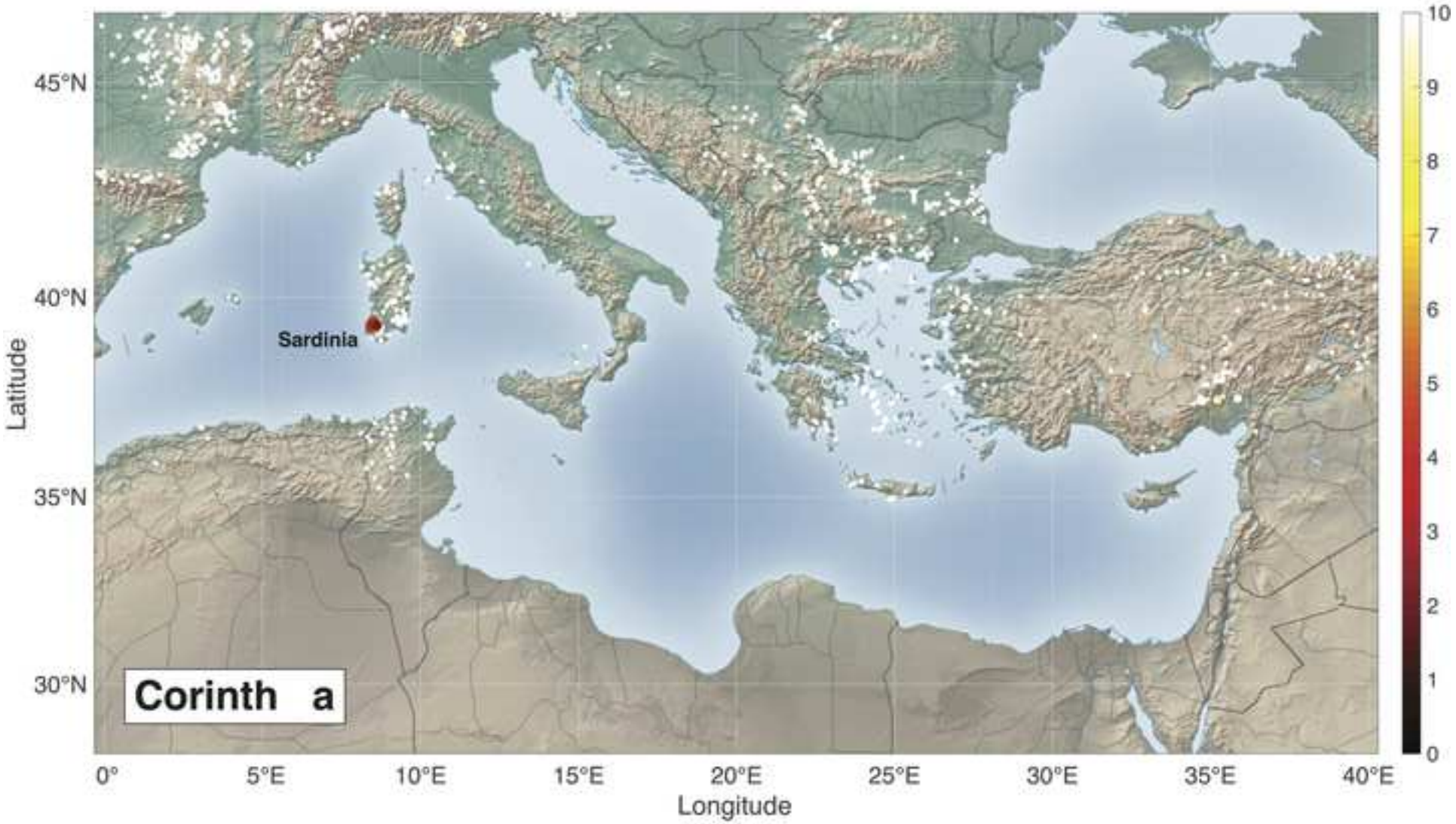

Figure 5b

Click here to access/download;Figure;Fig.2-05b Corinth _map.jpg

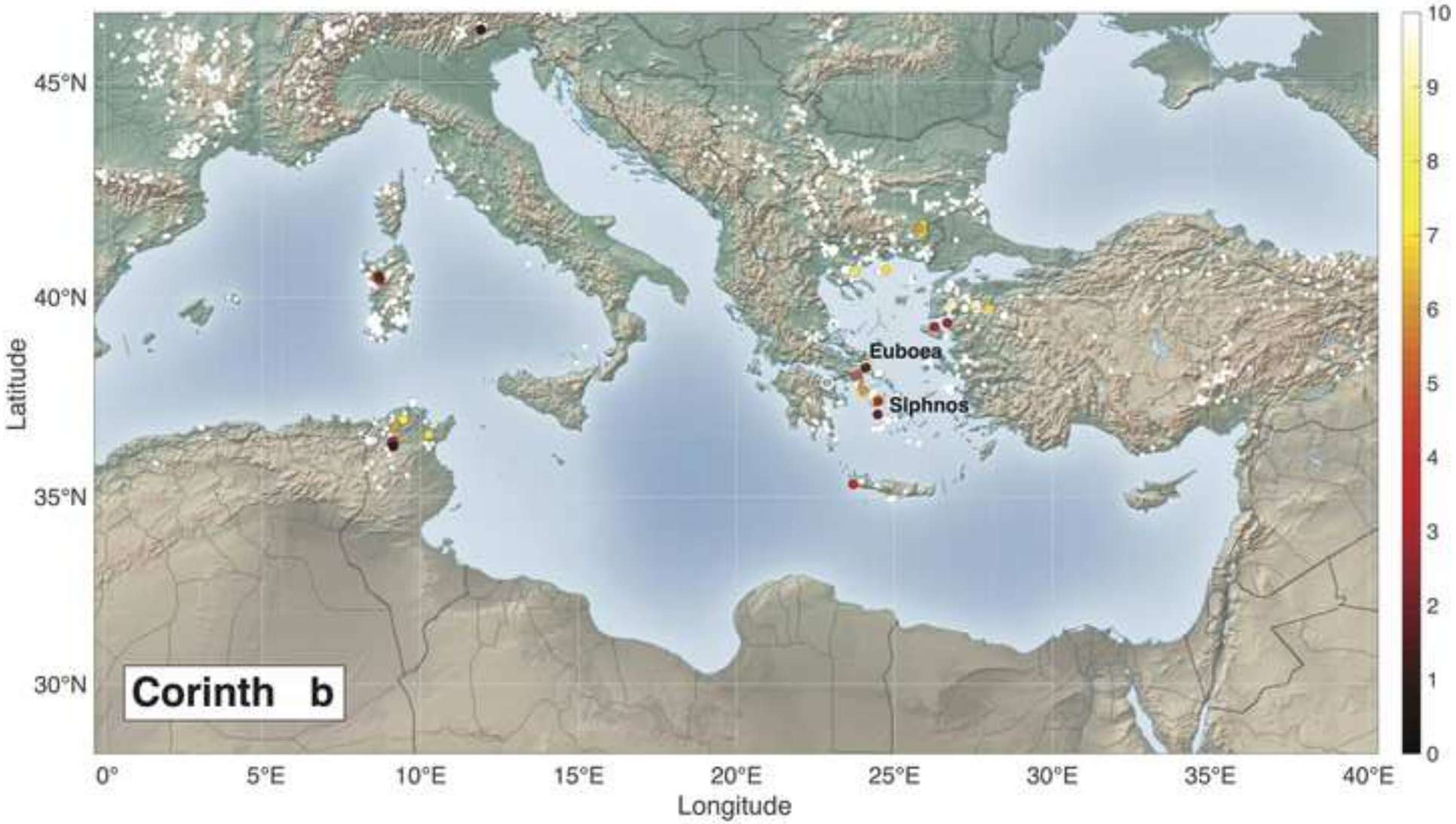

Figure 6a

Click here to access/download;Figure;Fig.2-06a Aegina_map.jpg

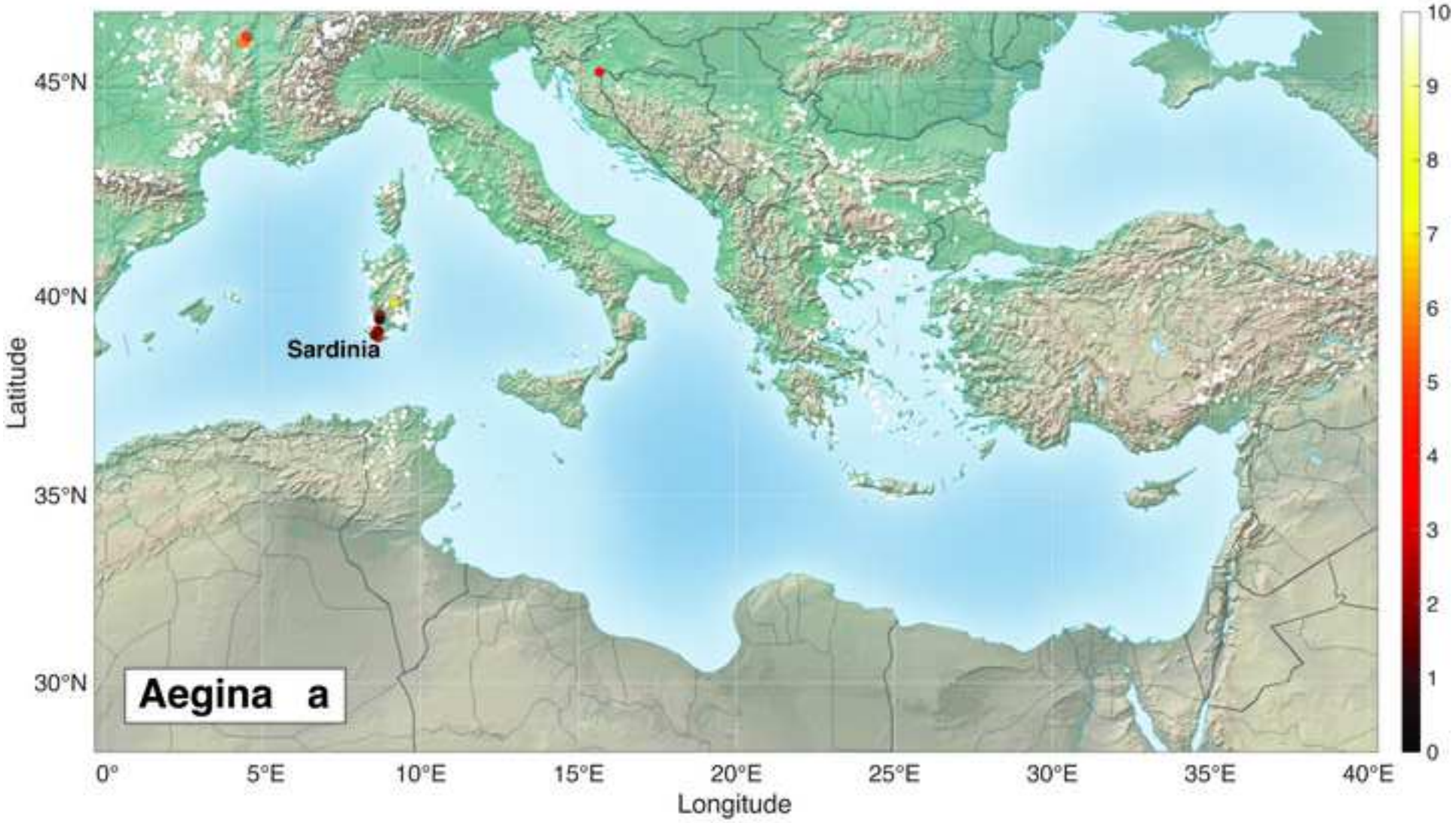

Figure 6b

Click here to access/download;Figure;Fig.2-06b Aegina_map.jpg

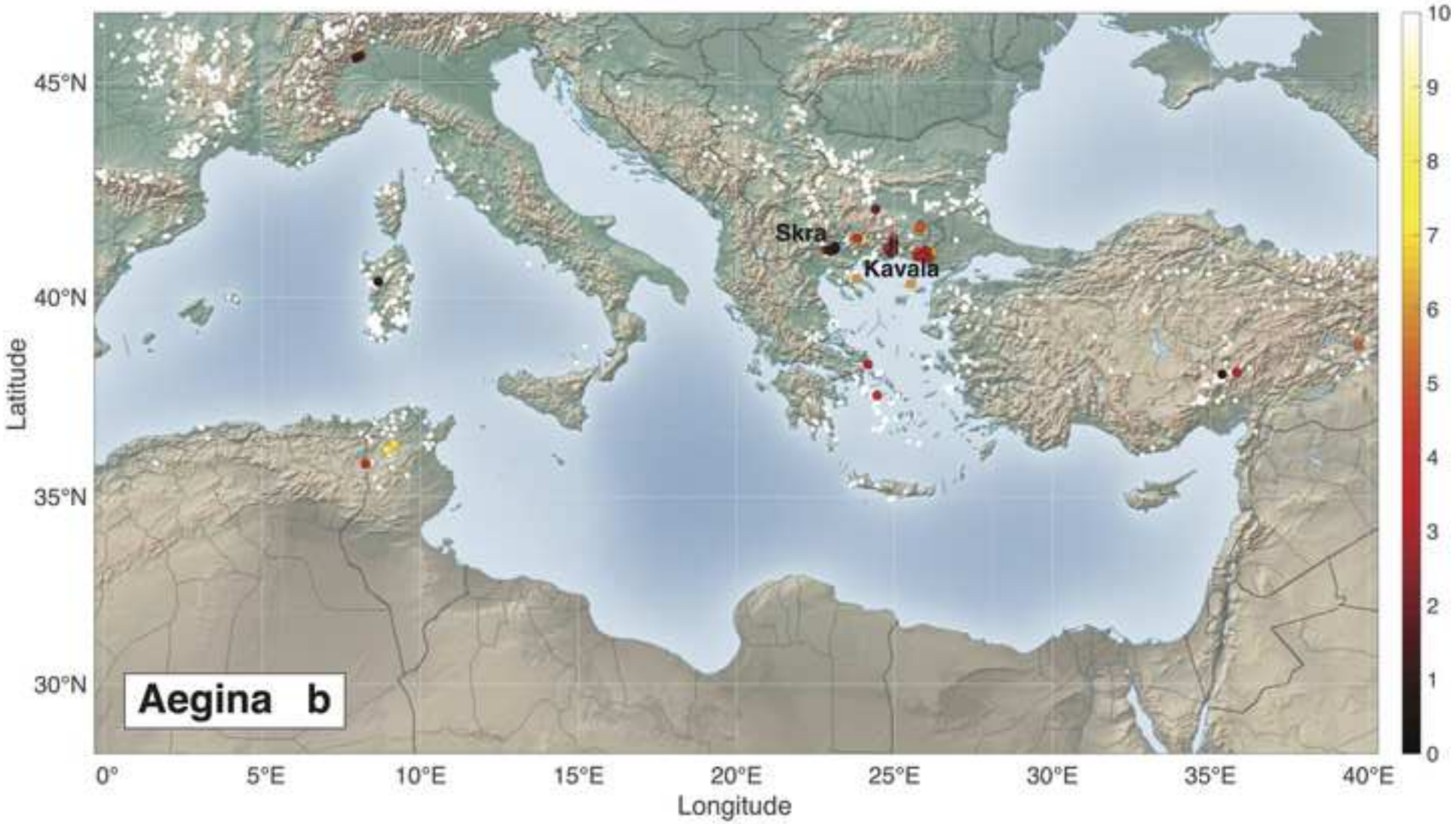

Figure 7a

Click here to access/download;Figure;Fig.2-07a Thasos_map.jpg

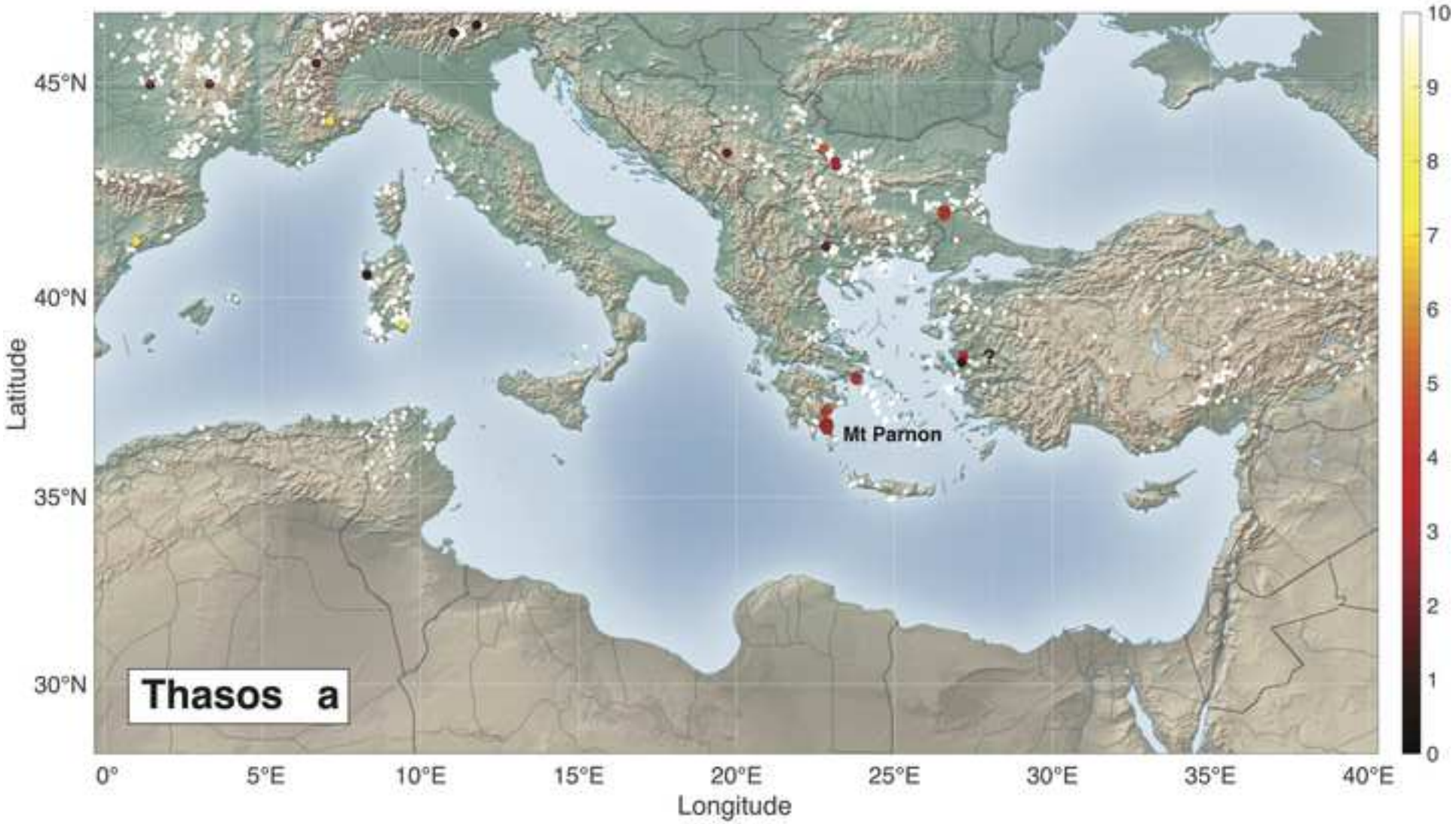

Figure 7b

Click here to access/download;Figure;Fig.2-07b Thasos_map.jpg

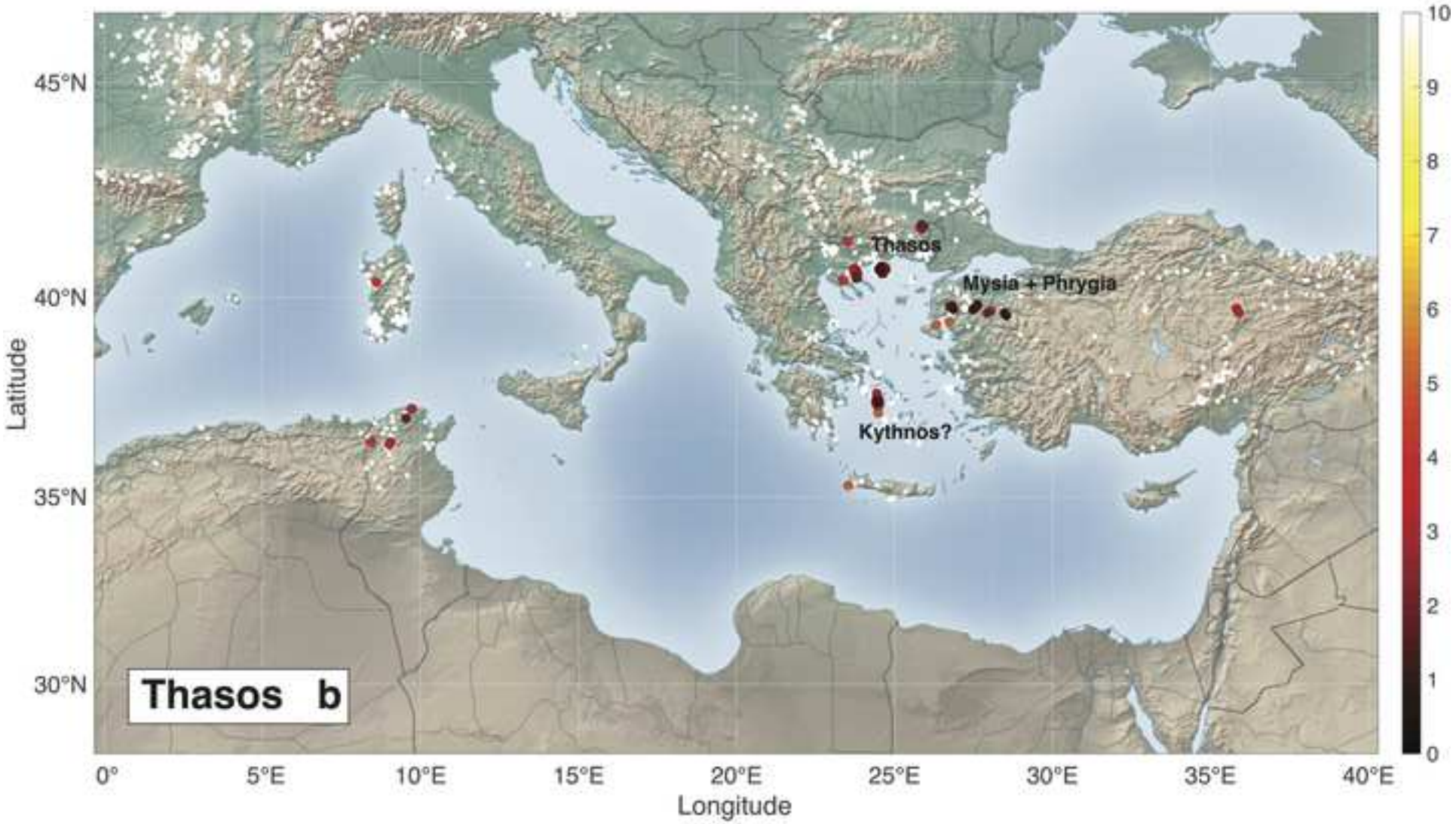

Figure 8a

Click here to access/download;Figure;Fig.2-08a Thrace_map.jpg

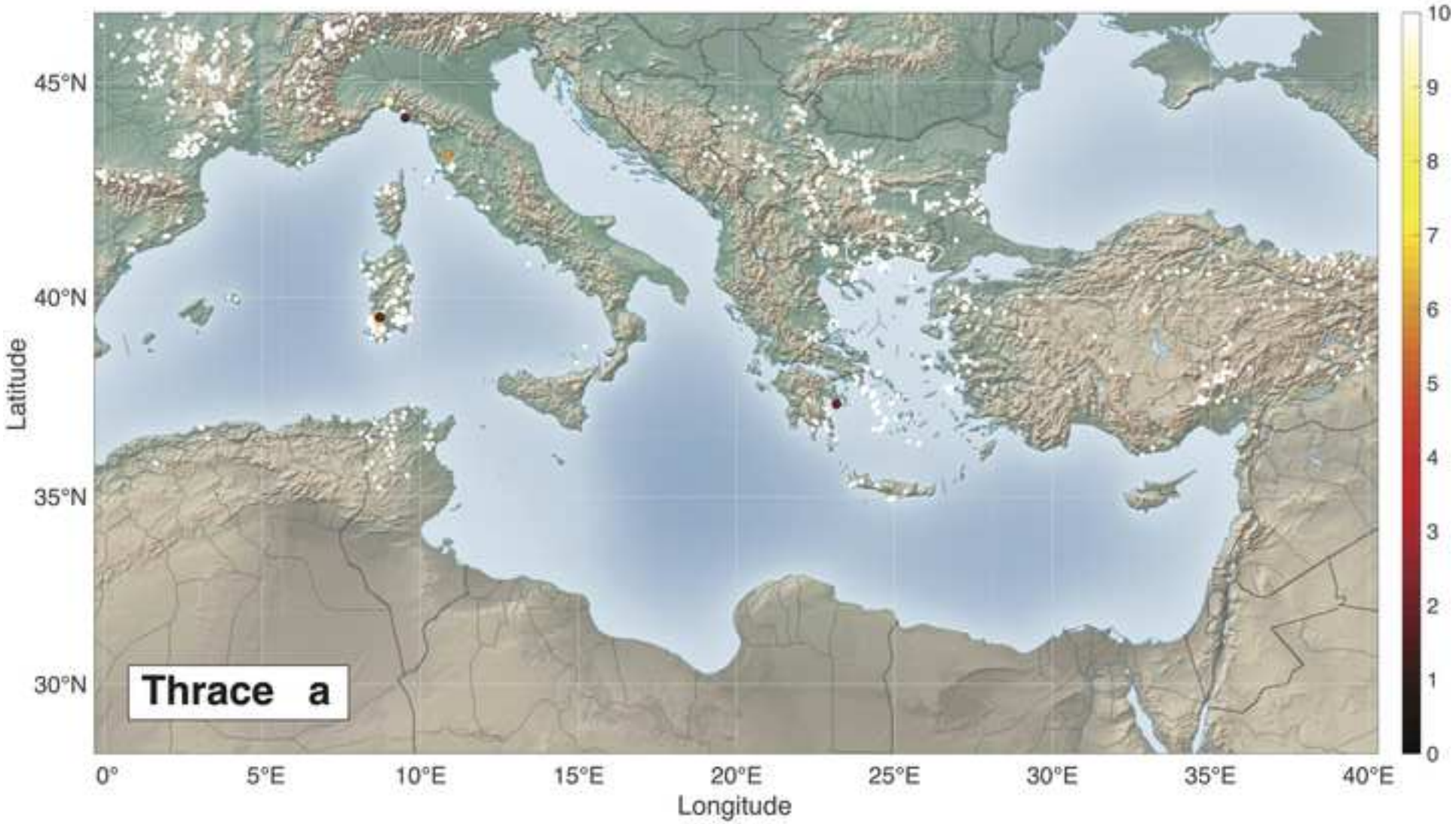

Figure 8b

Click here to access/download;Figure;Fig.2-08b Thrace_map.jpg

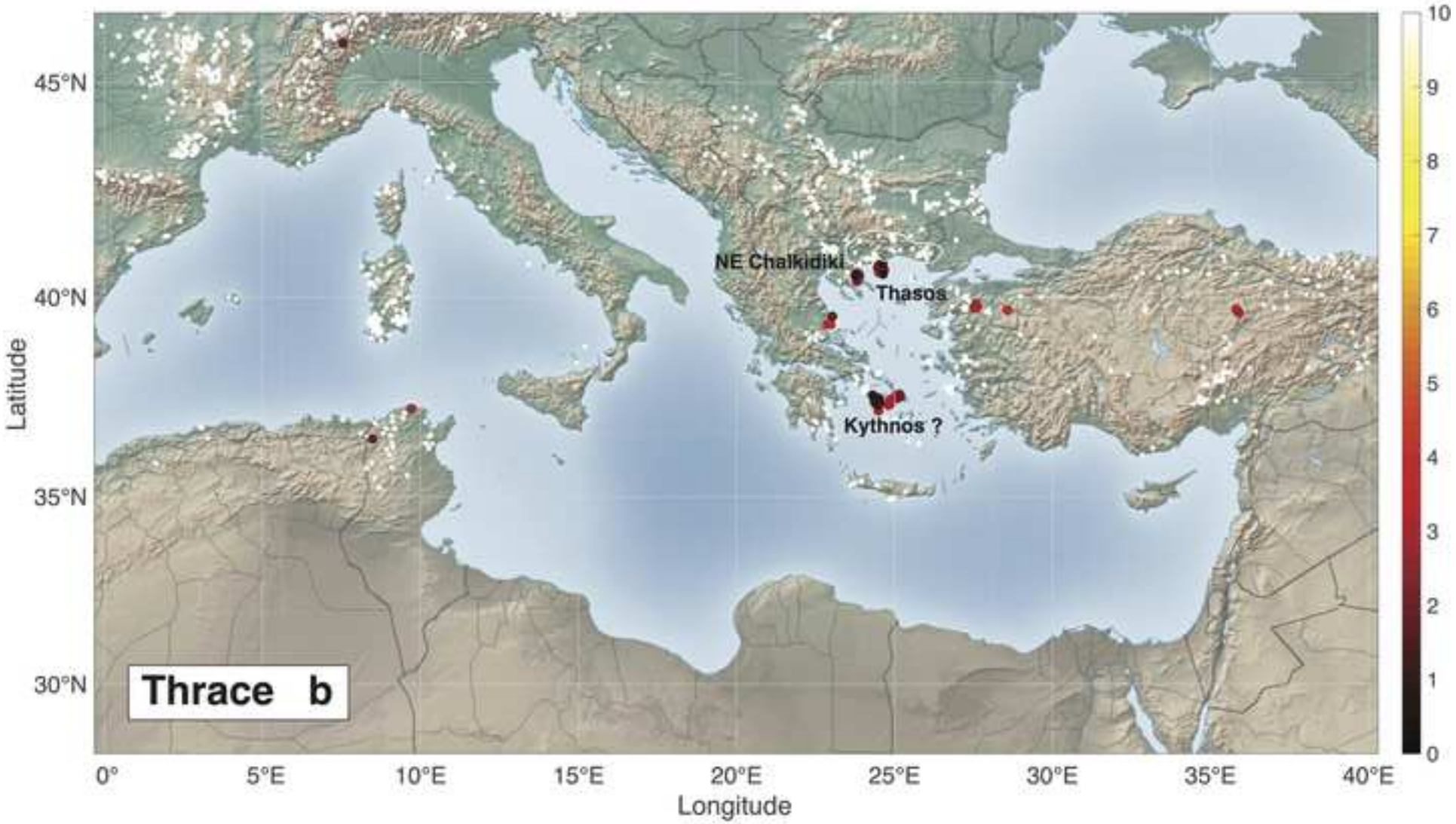

Figure 9a

Click here to access/download;Figure;Fig.2-09a Macedonia_map.jpg

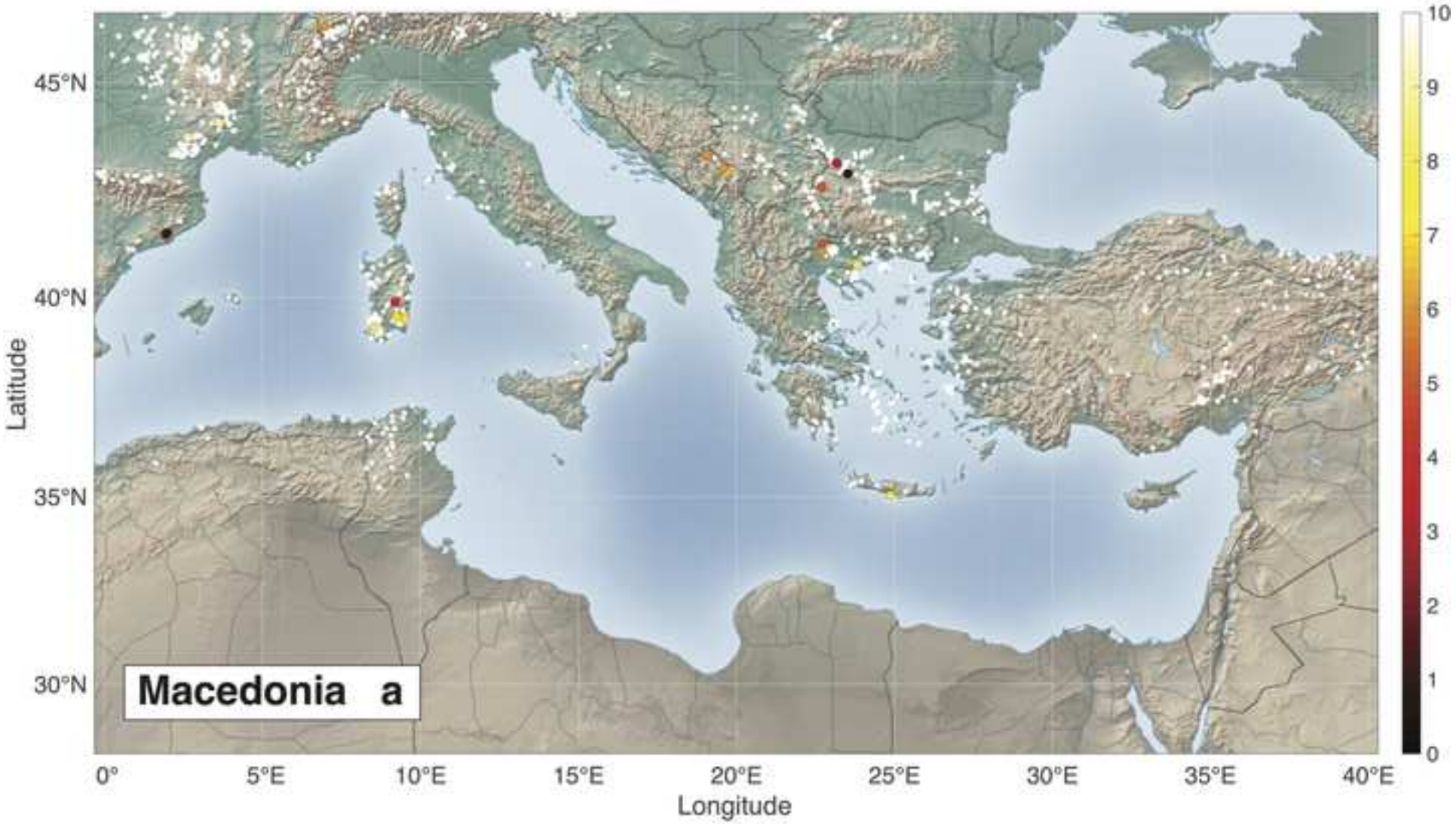

Figure 9b

Click here to access/download;Figure;Fig.2-09b Macedonia_map.jpg

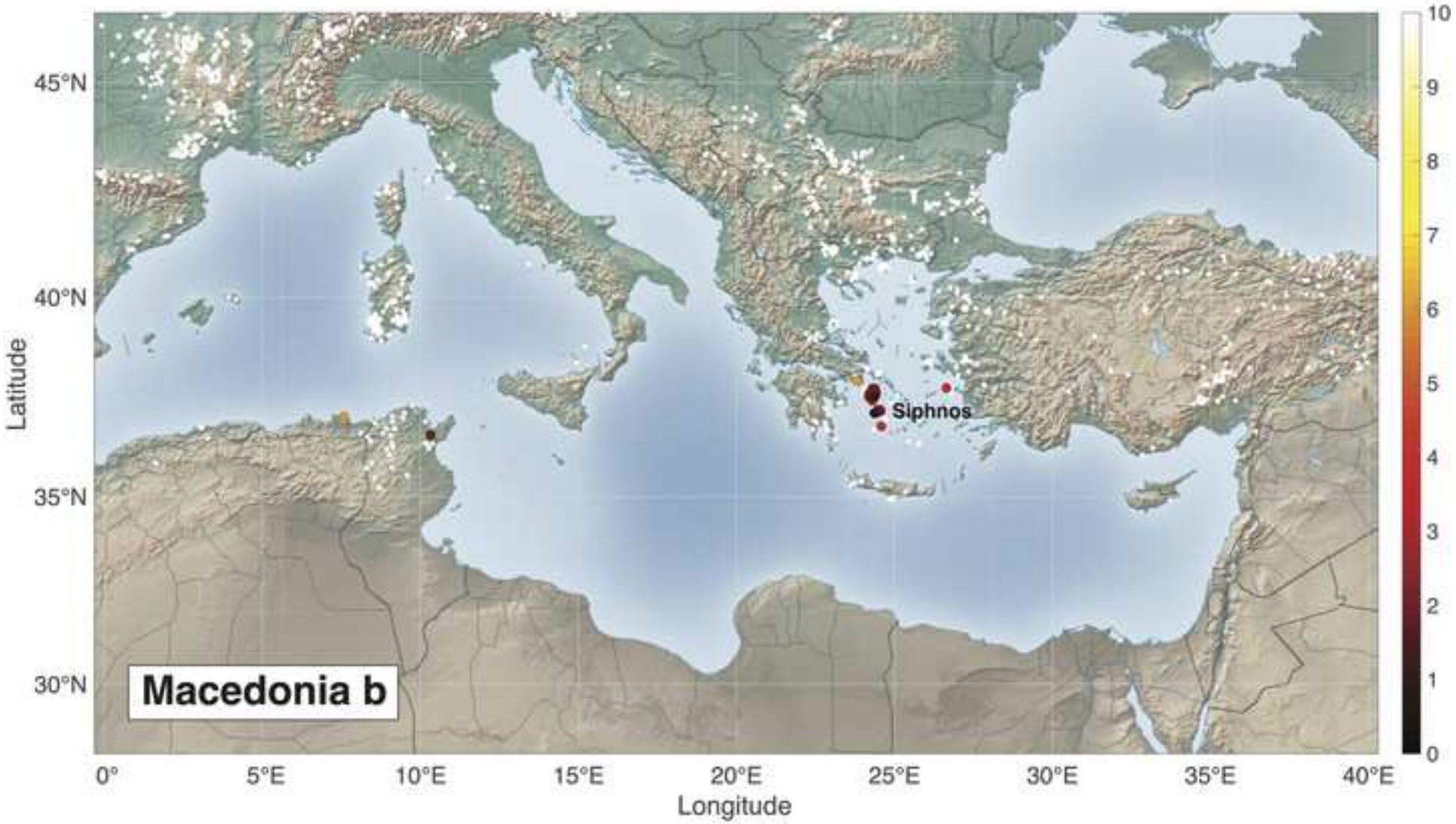

Figure 10a

Click here to access/download;Figure;Fig.2-10a Ptolemies_map.jpg

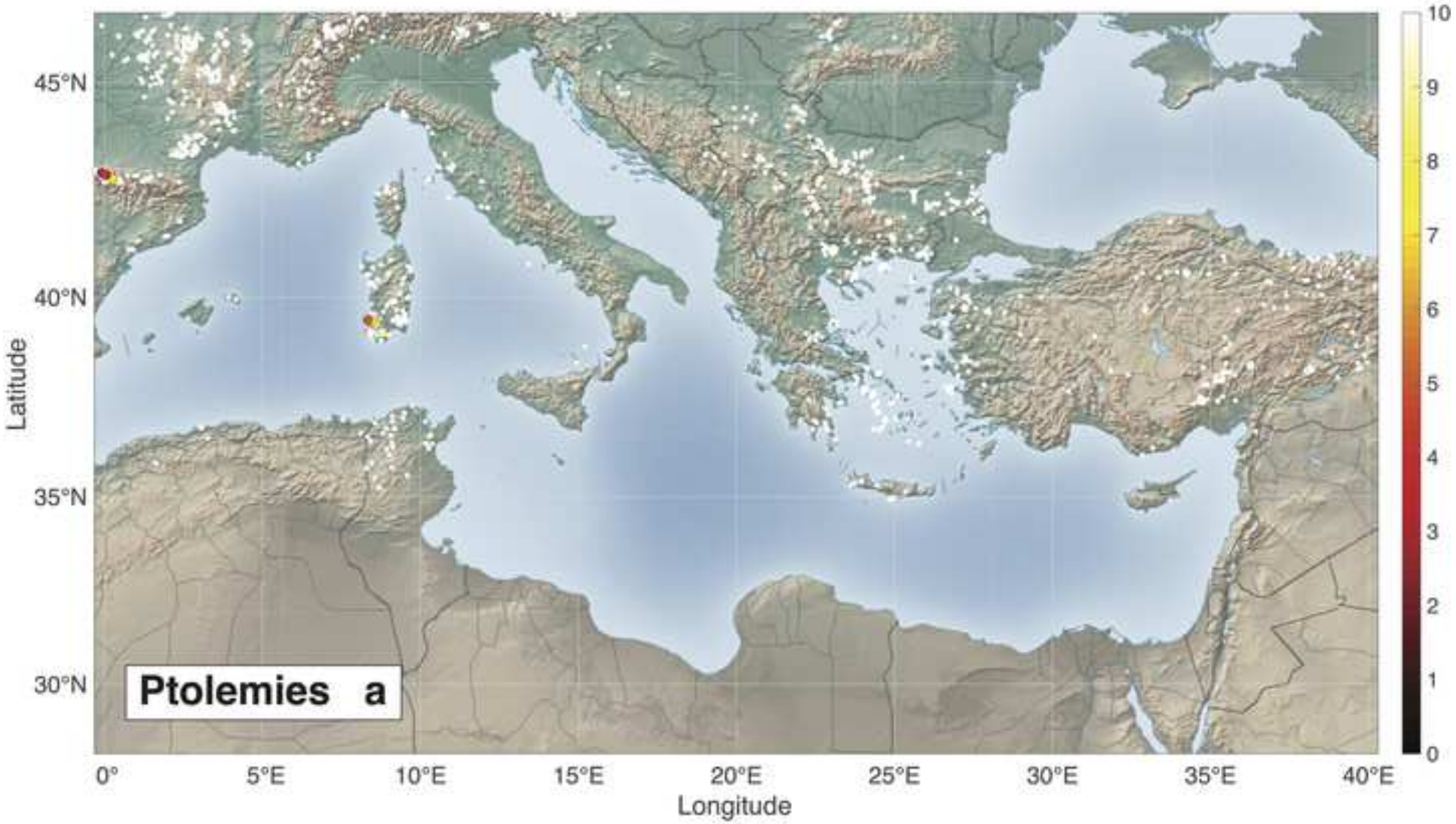

Figure 10b

Click here to access/download;Figure;Fig.2-10b Ptolemies_map.jpg